Commun. Comput. Phys.
doi: 10.4208/cicp.190809.141209a

Vol. **8**, No. 3, pp. 663-689
September 2010

Navier-Stokes Spectral Solver in a Finite Cylinder

F. Auteri*, M. Biava and L. Quartapelle

Politecnico di Milano, Dipartimento di Ingegneria Aerospaziale, Via La Masa 34, 20156 Milano, Italy.

Received 19 August 2009; Accepted (in revised version) 14 December 2009

Communicated by Jie Shen

Available online 20 April 2010

Abstract. A primitive variable spectral method for simulating incompressible viscous flows inside a finite cylinder is presented. One element of originality of the proposed method is that the radial discretization of the Fourier coefficients depends on the Fourier mode, its dimension decreasing with the increase of the azimuthal modal number. This principle was introduced independently by Matsushima and Marcus and by Verkley in polar coordinates and is adopted here for the first time to formulate a 3D cylindrical Galerkin projection method. A second element of originality is the use of a special basis of Jacobi polynomials introduced recently for the radial dependence in the solution of Dirichlet problems. In this basis the radial operators are represented by matrices of minimal sparsity — diagonal stiffness and tridiagonal mass — provided here in closed form for the first time, and lead to a Helmholtz operator characterized by a favorable condition number. Finally, a new method is presented for eliminating the singular behaviour of the solution originated by the rotation of the lid with respect to the cylindrical wall. Thanks to these elements, the resulting Navier-Stokes spectral solver guarantees the differentiability to any order of the solution in the entire computational domain and does not suffer from the time-step stability restriction occurring in spectral methods with a point clustering close to the axis. Several test examples are offered that demonstrate the spectral accuracy of the solution method under different representative conditions.

AMS subject classifications: 65N30, 65N35

Key words: Navier-Stokes equations, finite cylindrical domain, spectral methods, Jacobi and Legendre polynomials, primitive variables, projection method.

1 Introduction

To simulate the flow inside cylindrical cavities or along straight tubes of circular cross section the use of cylindrical coordinates is the natural choice and the adoption of a spec-

*Corresponding author. *Email address:* auteri@aero.polimi.it (F. Auteri)

tral discretization is particularly convenient when high accuracy is a major concern. In the last two decades several numerical schemes of this type have been developed for solving the incompressible Navier-Stokes equations to study the stability and investigate the transition of flows within cylindrical walls.

Focusing directly on fully 3D, i.e., not axisymmetric, flows, the first successful spectral methods for solving the equations in cylindrical coordinates were introduced by Moser et al. [1] and by Marcus [2] to simulate the flow between concentric cylinders of infinite axial extent. For the more challenging situation of a finite cylindrical gap the first spectral scheme was developed by Le Quéré and Pécheux to reproduce natural convection flows by means of Chebyshev polynomials and using the influence matrix technique [3].

Coming to cylindrical domains including the axis, a first attempt for the axially periodic case was done by Quartapelle and Verri who proposed an uncoupled Chebyshev method employing integral conditions for pressure [4]. Then, for the very important case of a finite cylinder, the spectral method of Lopez et al. must be mentioned [5]. It is a projection method representing the full 3D extension of the axisymmetric spectral solver developed by Lopez and Shen [6]. These methods stem from a Galerkin formulation of the underlying elliptic equations and employ the hierarchical bases of Legendre polynomials leading to matrices of very small bandwidth introduced by Shen in [7].

When the computational domain includes the axis or part of it, any spatial discretization is faced with the difficulty that the system of cylindrical variables entails a coordinate singularity at the axis, the so-called "pole" or "centre problem". In fact, there are regularity conditions on the Fourier expansion coefficients to be respected on the axis to guarantee the infinite differentiability of scalar and vector functions there, as clarified by the analysis of Lewis and Bellan [8]. For spectral methods their fulfillment can ensure the spectral accuracy of the computed solutions.

Methods have been proposed in the last years for dealing with the axis problem in spectral approximations for incompressible viscous flows inside cylindrical walls. Just to mention two examples, Fornberg introduced a method consisting in extending the radial variable also to negative values [9], see also [10, Sec. 6.2, p. 110] or [11, Chap. 11, p. 115], Speetjiens and Clercx described a Chebyshev collocation method for the vorticity-velocity equations resorting to the influence matrix technique [12].

From the mathematical viewpoint of solving elliptic equations, the occurrence of the singularity on the axis in cylindrical coordinates was addressed originally by Mercier and Raugel for a finite-element-based approximation [14]. In the context of spectral methods, the issue has been considered in the monograph [15, Sec. 3.4.1, p. 90] and a variational formulation of scalar elliptic equations based on weighted Sobolev spaces is described in the monograph of Bernardi et al. [16].

As a matter of fact, the difficulties associated with the pole can be actually turned into an opportunity when discretizing the problem by means of a spectral approximation. According to the analysis of [8] the Fourier components $u^m(r,z)$ of a differentiable scalar function $u(r,z,\phi)$ of the cylindrical coordinates (r,z,ϕ) must satisfy the following

conditions to be a regular function of $\mathbb{R}^3$:

$$u^m(r,z) = r^{|m|} U^m(r^2,z),$$

with the function $U^m(s,z)$, $s \geq 0$, being a regular function of its two variables. If these regularity conditions are not satisfied, the pole problem arises, since the numerical scheme provides an unwanted over-resolution near the cylinder axis which may severely limit the time step in the solution of evolutionary problems. On the other hand, the regularity conditions are helpful since they can be exploited to reduce the number of basis functions employed, by omitting the functions not satisfying them.

The first well conditioned basis that satisfies all the regularity conditions above and provides spectral accuracy has been proposed by Matsushima and Marcus [17] in the context of the solution of 2D Neumann boundary value problems, see also Verkley [18, 19]. This basis has also been employed recently by Boronski and Tuckerman in a pseudo-spectral method for the Navier-Stokes equations with the velocity field expressed in terms of poloidal and toroidal potentials [13]. A different approach has been adopted by Priymak and Miyazaki [20] who proposed a spectral Navier-Stokes solver with periodic boundary conditions along the cylinder axis satisfying regularity conditions on the axis by means of a suitable change of variable and employing a Chebyshev expansion in the radial direction.

Unfortunately, the condition numbers associated with Helmholtz operator grow as the fourth power of the degree for this basis. Moreover, its application to solve Dirichlet problems is unduly complicated. However, an important achievement of these works is that they have made explicit the advantage of using a spectral discretization for the radial variable that depends on the Fourier modal index. This implies the use of matrices of different order for representing the radial operators of different Fourier modes. Actually, this principle is not entirely new. It is in fact at the heart of the representation by spherical harmonics of functions defined over a sphere, with the number of associated Legendre functions required for the latitudinal description decreasing with the longitudinal frequency.

To exploit this idea for the Dirichlet problem in cylindrical coordinates a new Jacobi basis has been introduced to represent radial variations by Auteri and Quartapelle for Poisson and Helmholtz equations [21], that overcomes the disadvantages of that developed for the Neumann problem. The new basis leads to matrices for radial operators characterized by a minimal sparsity: for any Fourier mode, the stiffness matrix turns out to be diagonal and the mass matrix tridiagonal, and all their nonzero elements can be calculated in closed form, as described in the present paper. Moreover the condition number of the radial elliptic operator grows as the second power of the degree of the basis.

The aim of the present paper is to employ the new Jacobi basis to develop a spectral method for the simulation of incompressible viscous flows inside a cylinder. The solution algorithm for the primitive-variable Navier-Stokes equations is formulated according to the incremental fractional-step method of Guermond and Quartapelle [22] and extends

the Cartesian spectral method developed by Auteri and Parolini [23] to cylindrical domains of finite axial extent.

The paper is organized as follows. In Section 2, the incompressible Navier-Stokes problem is stated and the basic elements of the second-order incremental fractional-step method are recalled. In Section 3, the spectral approximation of elliptic equations in a cylindrical domain is described. In Section 4, the evaluation of the explicit terms, namely, gradient, divergence and nonlinear terms, in weak form is outlined. Section 5 describes an original analytical method for removing the singularity of the velocity boundary conditions when one lid of the cylindrical container or both rotates while the lateral surface is fixed. Section 6 contains the results of some numerical tests on the Navier-Stokes solver. The last section is devoted to the concluding remarks.

2 Navier-Stokes equations and projection method

This paper deals with the motion of a viscous fluid of uniform density inside a cylinder of finite axial extent, governed by the incompressible Navier-Stokes equations

$$\begin{cases} \dfrac{\partial \boldsymbol{u}}{\partial t} + (\boldsymbol{u}\cdot\boldsymbol{\nabla})\boldsymbol{u} - \nu\nabla^2\boldsymbol{u} + \boldsymbol{\nabla} p = \boldsymbol{f}(\boldsymbol{r},t), \qquad \boldsymbol{\nabla}\cdot\boldsymbol{u} = 0, \\ \boldsymbol{u}_{|\partial\Omega} = \boldsymbol{b}, \qquad \boldsymbol{u}_{|t=0} = \boldsymbol{u}_0, \end{cases} \tag{2.1}$$

where $\boldsymbol{u}$ is the velocity, $p = P/\overline{\rho}$ is the pressure per unit density of the fluid, ν is the kinematic viscosity and $\boldsymbol{f}(\boldsymbol{r},t)$ is an external force field (per unit mass) possibly acting on the fluid, for example the gravitational field. In the problem above, $\boldsymbol{b}(\boldsymbol{r}_{\partial\Omega},t)$, with $\boldsymbol{r}_{\partial\Omega} \in \partial\Omega$, represents the velocity prescribed on the boundary and $\boldsymbol{u}_0(\boldsymbol{r})$ is the initial velocity field. The domain Ω is a finite cylinder of radius a and height $2h$ so that its boundary $\partial\Omega$ consists of the lateral cylindrical surface $a\times[-h,h]\times[0,2\pi)$, and of the top and bottom circular lids $[0,a]\times\{\pm h\}\times[0,2\pi)$.

The Navier-Stokes problem (2.1) is solved by means of the second-order BDF incremental projection method described in [22] with reference to a finite element spatial discretization and assuming a semi-implicit treatment of the nonlinear term. The unconditional stability and the time convergence of that integration scheme has been demonstrated by Guermond [24]. In the spectral discretization of interest here, the nonlinear term is taken into account only explicitly by means of linear extrapolation for approximating the velocity field at the new time level, so that a conditionally stable scheme is obtained, with the time-step size limited by a suitable stability restriction.

The fractional-step approach is based on splitting the time advancement of the momentum equation in two distinct phases or sub-steps. The first sub-step consists in the following viscous problem for the vector unknown $\boldsymbol{u}^{k+1}$:

$$\begin{cases} \dfrac{3\boldsymbol{u}^{k+1} - 4\boldsymbol{u}^k + \boldsymbol{u}^{k-1}}{2\Delta t} - \nu\nabla^2\boldsymbol{u}^{k+1} = \boldsymbol{f}^{k+1} - \boldsymbol{\nabla} p_\star^k - (\boldsymbol{u}_\star^{k+1}\cdot\boldsymbol{\nabla})\boldsymbol{u}_\star^{k+1}, \\ \boldsymbol{u}^{k+1}{}_{|\partial\Omega} = \boldsymbol{b}^{k+1}, \end{cases} \tag{2.2}$$

where $\boldsymbol{f}^{k+1}=\boldsymbol{f}(\boldsymbol{r},t_{k+1})$, and $\boldsymbol{b}^{k+1}=\boldsymbol{b}(\boldsymbol{r}_{\partial\Omega},t_{k+1})$. Here the extrapolated velocity and pressure fields are defined respectively by

$$\boldsymbol{u}_\star^{k+1}=\begin{cases}\boldsymbol{u}_0, & \text{for } k=0,\\ 2\boldsymbol{u}^k-\boldsymbol{u}^{k-1}, & \text{for } k\geq 1,\end{cases} \tag{2.3}$$

and

$$p_\star^k=\begin{cases}p_0, & \text{for } k=0,\\ 3p^1-2p_0, & \text{for } k=1,\\ \frac{1}{6}(14p^2-11p^1+3p_0), & \text{for } k=2,\\ \frac{1}{3}(7p^k-5p^{k-1}+p^{k-2}), & \text{for } k\geq 3,\end{cases} \tag{2.4}$$

with p_0 denoting an initial pressure field which must be provided or calculated insofar as the incremental method is employed since the first time step.

The second sub-step consists in projecting $\boldsymbol{u}^{k+1}$ onto the space of the divergenceless vector fields that are tangent to the boundary $\partial\Omega$ and can be formulated as the following Poisson problem for pressure

$$\begin{cases}-\nabla^2(p^{k+1}-p^k)=-\dfrac{3}{2\Delta t}\boldsymbol{\nabla}\cdot\boldsymbol{u}^{k+1},\\ \partial_n(p^{k+1}-p^k)\big|_{\partial\Omega}=0,\end{cases} \tag{2.5}$$

subject to a homogeneous Neumann boundary condition. A review of projection methods is given by Guermond et al. [25].

3 Discretized equations in cylindrical coordinates

3.1 Helmholtz equation for velocity

At each viscous step one has to solve the vector Helmholtz equation

$$\left(-\nabla^2+\gamma\right)\boldsymbol{u}=\boldsymbol{f}(r,z,\phi), \tag{3.1}$$

in cylindrical coordinates (r,z,ϕ), with $\gamma>0$, supplemented by the Dirichlet condition

$$\boldsymbol{u}(r,z,\phi)_{|\partial\Omega}=\boldsymbol{b}(r,z,\phi),$$

where $\boldsymbol{b}$ is defined on the entire boundary $\partial\Omega$ of the cylindrical domain. The domain of definition goes all around the z-axis, that is, $0\leq\phi<2\pi$. Since we are interested only in *real* vector fields, the velocity $\boldsymbol{u}(r,z,\phi)$ will be represented by means of a real discrete Fourier expansion

$$\begin{aligned}\boldsymbol{u}(r,z,\phi)=&\boldsymbol{u}^0(r,z)+2\sum_{m=1}^{N-1}\Big(\boldsymbol{u}^m(r,z)\cos(m\phi)-\boldsymbol{u}^{-m}(r,z)\sin(m\phi)\Big)\\ &+u_z^N(r,z)\cos(N\phi)\,\hat{\boldsymbol{z}}.\end{aligned} \tag{3.2}$$

This particular form of the Fourier expansion is requested by the FFT library adopted for the implementation of the algorithm. The Fourier vector coefficients are

$$\boldsymbol{u}^m(r,z)=u_r^m(r,z)\hat{\boldsymbol{r}}+u_\phi^m(r,z)\hat{\boldsymbol{\phi}}+u_z^m(r,z)\hat{\boldsymbol{z}}, \tag{3.3}$$

with $\hat{\boldsymbol{r}}$, $\hat{\boldsymbol{\phi}}$ and $\hat{\boldsymbol{z}}$ denoting the unit vectors of the cylindrical coordinate system.

Introducing the expansions for $\boldsymbol{u}$ and $\boldsymbol{f}$ into the Helmholtz equation (3.1) and equating similar terms with respect to the angular basis functions, we obtain a series of systems of equations. Each system is uncoupled from the others and reads, for any integer m,

$$(-\boldsymbol{\partial}_m^2+\gamma)\begin{pmatrix}u_r^m\\ u_\phi^{-m}\\ u_z^m\end{pmatrix}=\begin{pmatrix}f_r^m(r,z)\\ f_\phi^{-m}(r,z)\\ f_z^m(r,z)\end{pmatrix}, \tag{3.4}$$

where

$$\boldsymbol{\partial}_m^2=\begin{pmatrix}\partial_m^2-\dfrac{1}{r^2} & \dfrac{2m}{r^2} & 0\\ \dfrac{2m}{r^2} & \partial_m^2-\dfrac{1}{r^2} & 0\\ 0 & 0 & \partial_m^2\end{pmatrix},\quad\text{with}\quad \partial_m^2=\frac{1}{r}\frac{\partial}{\partial r}\Big(r\frac{\partial}{\partial r}\Big)+\frac{\partial^2}{\partial z^2}-\frac{m^2}{r^2}. \tag{3.5}$$

For $m=0$ the system consists of three uncoupled equations since the vector differential operator $\boldsymbol{\partial}_0^2$ is diagonal. For any $|m|\geq 1$, we have a series of systems each consisting of a subsystem of two coupled equations for the radial and angular components of velocity plus an uncoupled equation for the axial component.

3.2 Uncoupling the cylindrical components

The z component of the vector field $\boldsymbol{u}^m$ being uncoupled, we focus our attention on the algorithm for the uncoupled solution of the other two components, namely, we consider the two-component vector unknown

$$\boldsymbol{u}^m(r,z)=u_r^m(r,z)\hat{\boldsymbol{r}}+u_\phi^m(r,z)\hat{\boldsymbol{\phi}},\quad -\infty<m<\infty, \tag{3.6}$$

for which the system above reduces to

$$(-\boldsymbol{\partial}_m^2+\gamma)\begin{pmatrix}u_r^m\\ u_\phi^{-m}\end{pmatrix}=\begin{pmatrix}f_r^m(r,z)\\ f_\phi^{-m}(r,z)\end{pmatrix},\quad\text{with now}\quad \boldsymbol{\partial}_m^2=\begin{pmatrix}\partial_m^2-\dfrac{1}{r^2} & \dfrac{2m}{r^2}\\ \dfrac{2m}{r^2} & \partial_m^2-\dfrac{1}{r^2}\end{pmatrix}. \tag{3.7}$$

Let us introduce the following symmetric and orthonormal transformation matrix

$$\boldsymbol{Q}=\frac{1}{\sqrt{2}}\begin{pmatrix}1 & 1\\ 1 & -1\end{pmatrix}, \tag{3.8}$$

whose action on the Fourier modes is defined by

$$\begin{pmatrix} f_1^{m-1} \\ f_2^{m+1} \end{pmatrix} = \boldsymbol{Q} \begin{pmatrix} f_r^m \\ f_\phi^{-m} \end{pmatrix}, \quad \text{and} \quad \begin{pmatrix} u_r^m \\ u_\phi^{-m} \end{pmatrix} = \boldsymbol{Q} \begin{pmatrix} u_1^{m-1} \\ u_2^{m+1} \end{pmatrix}. \tag{3.9}$$

By left multiplying the system (3.7) for $m \neq 0$ by $\boldsymbol{Q}$ and exploiting the properties of $\boldsymbol{Q}$, we obtain

$$\boldsymbol{Q}(-\partial_m^2 + \gamma)\, \boldsymbol{Q} \begin{pmatrix} u_1^{m-1} \\ u_2^{m+1} \end{pmatrix} = \boldsymbol{Q} \begin{pmatrix} f_r^m(r,z) \\ f_\phi^{-m}(r,z) \end{pmatrix}, \tag{3.10}$$

and

$$\boldsymbol{Q}\partial_m^2 \boldsymbol{Q} = \begin{pmatrix} \partial_{m-1}^2 & 0 \\ 0 & \partial_{m+1}^2 \end{pmatrix}. \tag{3.11}$$

In other words, the matrix $\boldsymbol{Q}$ defines the following transformation $\mathbb{Q}$ of the full set of the vector Fourier modes

$$\left\{ \begin{pmatrix} u_1^m \\ u_2^m \end{pmatrix},\ m = 0, \pm 1, \pm 2, \cdots \right\} = \mathbb{Q} \left\{ \begin{pmatrix} u_r^m \\ u_\phi^m \end{pmatrix},\ m = 0, \pm 1, \pm 2, \cdots \right\}. \tag{3.12}$$

3.3 Uncoupled scalar Dirichlet problem

The transformation $\mathbb{Q}$ uncouples the system (3.7). The Helmholtz equation for the velocity vector (3.1) reduces to three uncoupled scalar equations for the velocity components u_χ^m, $\chi = 1,2,3$, with the understanding that $u_3 \equiv u_z$, that will be written as

$$(-\partial_m^2 + \gamma)\, u^m = f^m(r,z). \tag{3.13}$$

Eq. (3.13) is supplemented by Dirichlet boundary conditions, obtained introducing the truncated Fourier expansion of the boundary data

$$u^m(a,z) = b_{\mathrm{c}}^m(z), \qquad |z| \leq h, \tag{3.14a}$$

$$u^m(r,\mp h) = b_{\mathrm{b,t}}^m(r), \qquad 0 \leq r \leq a, \tag{3.14b}$$

for the modal unknown $u^m(r,z)$. Here $b_{\mathrm{c}}^m(z)$, with $|z| \leq h$, denotes the Dirichlet data for the Fourier components m on the outer side, while $b_{\mathrm{b}}^m(r)$ and $b_{\mathrm{t}}^m(r)$, with $0 \leq r \leq a$, denote those on the bottom and top sides.

To represent the modal unknown $u^m(r,z)$, with $-N+1 \leq m \leq N$, we first introduce the dimensionless variables $\rho = r/a$, with $0 < \rho \leq 1$, and $\zeta = z/h$, with $|\zeta| \leq 1$, and indicate the new unknown $\tilde{u}^m(\rho,\zeta) = u^m(r,z)$ by the same symbol u, as $u^m(\rho,\zeta)$. The new modal unknown $u^m(\rho,\zeta)$ is given the spectral representation employed in [21] for the solution of Dirichlet problems. One first introduces the polynomials in the mapped variable $s = 2\rho^2 - 1$, for $m \geq 0$,

$$P_0^{\star m}(s) = 1, \tag{3.15a}$$

$$P_i^{\star m}(s) = \frac{1-s}{2} P_{i-1}^{(1,m)}(s), \quad i = 1,2,\cdots, \tag{3.15b}$$

where $P_i^{(\alpha,\beta)}(s)$, $-1\le s\le 1$, denotes the Jacobi polynomials. Then, one introduces the expansion functions

$$Q_i^m(s)\equiv\Big(\frac{1+s}{2}\Big)^{m/2}P_i^{\star m}(s),\qquad i=0,1,2,\cdots, \tag{3.16}$$

as well as their counterparts dependent on the dimensionless radial variable ρ

$$B_i^m(\rho)\equiv Q_i^m\big(2\rho^2-1\big)=\rho^m P_i^{\star m}\big(2\rho^2-1\big). \tag{3.17}$$

For each value of m, only one basis function assumes nonhomogeneous values on the outer radius thus enabling to easily impose Dirichlet boundary conditions by means of a lifting.

Then, the axial variations when Dirichlet conditions apply are represented by employing the basis $\{L_j^*(\zeta)\}$, $-1\le\zeta\le 1$, introduced by Shen [7] defined as

$$L_0^*(\zeta)=1,\qquad L_1^*(\zeta)=\frac{\zeta}{\sqrt{2}}, \tag{3.18a}$$

$$L_n^*(\zeta)=\frac{L_{n-2}(\zeta)-L_n(\zeta)}{\sqrt{2(2n-1)}},\quad n\ge 2. \tag{3.18b}$$

This basis contains linear combinations of two Legendre polynomials which vanish at the extremes $\zeta=\pm 1$ to satisfy homogeneous Dirichlet conditions.

The spectral expansion to $u^m(\rho,\zeta)$ is obtained by the double series

$$u^m(\rho,\zeta)=\sum_{i=0}^{N-|m|}B_i^{|m|}(\rho)\,u_{i;j}^m\,L_j^*(\zeta)\overline{\sum_{j=0}^{J}}, \tag{3.19}$$

where the inverted summation symbol is used to denote the sum over the second summation index. Notice that different expansion functions are used to express the dependence of each Fourier component $u^m(\rho,\zeta)$ on the radial variable ρ. The number of involved functions decreases with m, going from $N+1$, for the first component with $m=0$, to only 1, for the last Fourier component with $m=N$. Correspondingly, the rectangular array of the expansion coefficients

$$U^m=\{u_{i;j}^m,\ 0\le i\le N-|m|;\ 0\le j\le J\}, \tag{3.20}$$

will be of dimensions $(N-|m|+1)\times(J+1)$, with a number of rows dependent on the Fourier modal index m.

Introducing this expansion in the Galerkin counterpart of Eq. (3.13) and choosing the weighting function $v(\rho,\zeta)$ as the product $B_i^{|m|}(\rho)\,L_j^*(\zeta)$ of the same basis functions used to expand the solution, the weak formulation leads to the following system of equations

$$\big(a^{-2}D_{\boxed{m}}+\gamma M_{\boxed{m}}\big)U^mM+M_{\boxed{m}}U^mDh^{-2}=G^m+\langle\text{B.I.}\rangle^m. \tag{3.21}$$

The special subscript used in $D_{\boxed{m}}$ and $M_{\boxed{m}}$ is to hallmark that the order of the corresponding square matrix is dependent on the Fourier index m. The boundary term $\langle \text{B.I.} \rangle^m$ will disappear when the Dirichlet boundary condition will be imposed by means of a lifting, see below. The matrices occurring in this system are defined as follows:

$$D_{\boxed{m}i,i'} = \int_{-1}^{1} \left[4\left(\frac{1+s}{2}\right) \frac{dQ_i^m(s)}{ds} \frac{dQ_{i'}^m(s)}{ds} + \frac{m^2}{4} \left(\frac{1+s}{2}\right)^{-1} Q_i^m(s) Q_{i'}^m(s) \right] ds, \tag{3.22}$$

$$M_{\boxed{m}i,i'} = \frac{1}{4} \int_{-1}^{1} Q_i^m(s) Q_{i'}^m(s) ds, \tag{3.23}$$

with $0 \le (i,i') \le N-m$, for the operators associated with the radial variable r. Matrix $D_{\boxed{m}}$ is diagonal [21] and its nonzero elements are defined by

$$D_{\boxed{m}i,i} = \begin{cases} m, & \text{for } i=0, \\ \dfrac{2i^2}{2i+m}, & \text{for } i \ge 1, \end{cases} \tag{3.24}$$

while matrix $M_{\boxed{m}}$ is symmetric tridiagonal [21] and its nonzero elements are defined by

$$M_{\boxed{m}i,i} = \begin{cases} \dfrac{1}{2(m+1)}, & \text{for } i=0, \\ \dfrac{i^2}{(2i+m-1)(2i+m)(2i+m+1)}, & \text{for } i \ge 1, \end{cases} \tag{3.25a}$$

$$M_{\boxed{m}i,i+1} = \begin{cases} \dfrac{1}{2(m+1)(m+2)}, & \text{for } i=0, \\ \dfrac{-i(i+1)}{2(2i+m)(2i+m+1)(2i+m+2)}, & \text{for } i \ge 1. \end{cases} \tag{3.25b}$$

The tridiagonal character of the mass matrix $M_{\boxed{m}}$ follows from the definition of the basis functions $Q_i^m(s)$ and from the orthogonality of the Jacobi polynomials $P_i^{(1,m)}(s)$

$$\int_{-1}^{1} (1-s)(1+s)^m P_i^{(1,m)}(s) P_k^{(1,m)}(s) ds = \frac{2^{m+2}(i+1)}{(2i+m+2)(i+m+1)} \delta_{i,k}, \tag{3.26}$$

with $i,k \ge 0$. The values of the nonzero elements of the mass matrix are obtained using this relation. The diagonal character of the stiffness matrix $D_{\boxed{m}}$ can be proved by starting with the integral of the weak equation before integrating by parts and using the Jacobi differential equation

$$(1-s^2) \frac{d^2 P_i^{(1,m)}(s)}{ds^2} + [m-1-(m+3)s] \frac{dP_i^{(1,m)}(s)}{ds} + i(i+m+2) P_i^{(1,m)}(s) = 0, \tag{3.27}$$

similarly to what suggested for the spherical case by P. W. Livermore in a private communication (2008).

On the other side, the matrices D and M for the operators in the axial variable are defined by

$$D_{j,j'}=\int_{-1}^{1}\frac{dL_j^*(\zeta)}{d\zeta}\frac{dL_{j'}^*(\zeta)}{d\zeta}d\zeta,\quad\text{and}\quad M_{j,j'}=\int_{-1}^{1}L_j^*(\zeta)L_{j'}^*(\zeta)d\zeta. \tag{3.28}$$

Matrix D is the identity matrix but for its first diagonal element which is zero: $D_{0,0}=0$. Matrix M is symmetric pentadiagonal. The elements of the array G^m on the right-hand side are defined by

$$g_{i;j}^m=\frac{1}{4}\int_{-1}^{1}\int_{-1}^{1}Q_i^{|m|}(s)f^m\left(a\left(\tfrac{1+s}{2}\right)^{1/2},h\zeta\right)L_j^*(\zeta)dsd\zeta. \tag{3.29}$$

3.4 Lifting of the Dirichlet condition

The nonhomogeneous Dirichlet value $b^m(\ell)$ is taken into account by means of a lifting, a classical procedure for making the boundary conditions homogeneous. The need of a lifting for developing multidimensional spectral solvers achieving a complete variable separation at the level of the spectral expansion coefficients is described in detail for a 3D rectangular domain in [26].

For the considered problem, the lifting of nonzero Dirichlet boundary values leads to the following linear system of discrete equations

$$\left(a^{-2}D_{\boxed{m}}+\gamma M_{\boxed{m}}\right)U^mM+M_{\boxed{m}}U^mh^{-2}=G^m, \tag{3.30}$$

where the matrices $D_{\boxed{m}}, M_{\boxed{m}}$ and M denote the lifted counterpart of the matrices $D_{\boxed{m}}, M_{\boxed{m}}$ and M, and similarly the array U^m denotes the lifted version of the unknown U^m and the array G^m is the right-hand side of the lifted system including the effect of the lifting. The linear system is solved by double diagonalization. The diagonalization on the left requires to solve generalized symmetric eigenvalue problems for the matrix pairs $(D_{\boxed{m}}, M_{\boxed{m}})$, $m=0,1,\cdots,N-1$, and is dealt with by the LAPACK routine `dsygvd`. The diagonalization on the right for banded symmetric matrix M is obtained by `dsbev`.

In Fig. 1 we report the condition numbers of the matrices $\left(a^{-2}D_{\boxed{m}}+\gamma M_{\boxed{m}}\right)$. The left plot shows the dependence of the condition number on Fourier modal index m for different truncations N, with $\gamma=1000$. The maximum condition number is found to correspond to the intermediate wavelengths of the truncated radial expansion. The plot on the right gives the maximum condition number for different truncations N and for $\gamma=1$ and $\gamma=10^3$. The maximum condition number grows quadratically with N, thus confirming the optimal conditioning of the proposed spectral approximation for the Dirichlet problem in cylindrical coordinates.

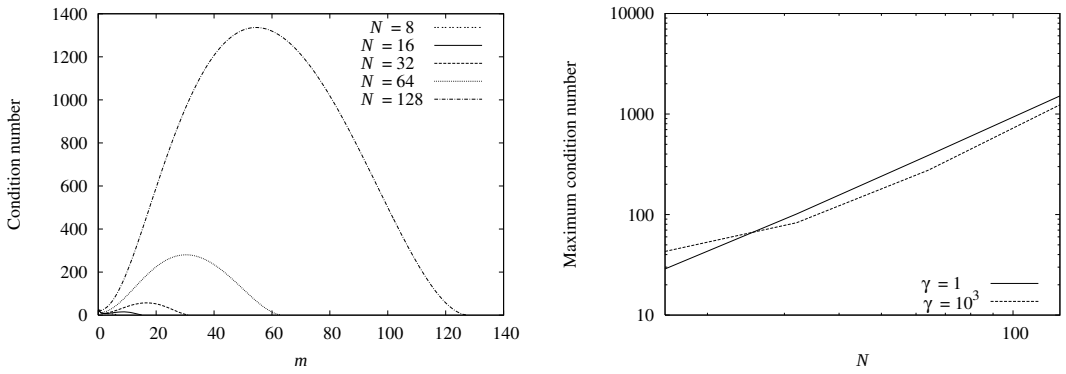

Figure 1: Condition numbers of matrices (3.30) of the Dirichlet problem. Left: distribution of the condition number with the Fourier modal index m for different truncations N and $\gamma=1000$. Right: maximum condition number as a function of the truncation N for different values of γ.

3.5 Poisson pressure equation

At each incompressible step the Poisson equation in cylindrical coordinates $-\nabla^2 p = q(r,z,\phi)$ must be solved, supplemented by the homogeneous Neumann boundary condition $(\partial_n p)_{|\partial\Omega}=0$. The source term $q=q(r,z,\phi)$ satisfies the compatibility condition $\int_\Omega q=0$, as a consequence of the imposition in the viscous step of the normal velocity boundary condition for incompressible flows. The unknown pressure field p is expanded in the finite Fourier series,

$$p(r,z,\phi)=p^0(r,z)+2\sum_{m=1}^{N-1}\left[p^m(r,z)\cos(m\phi)-p^{-m}(r,z)\sin(m\phi)\right] + p^N(r,z)\cos(N\phi), \tag{3.31}$$

where the presence of the last term for the component N without the coefficient 2 must be noticed. The equation for $p^m(r,z)$, with $-N+1\le m\le N$, is

$$-\partial_m^2 p^m = q^m(r,z), \tag{3.32}$$

and is supplemented by homogeneous Neumann conditions:

$$\partial_r p^m(a,z)=0, \qquad \text{for } |z|\le h, \tag{3.33a}$$
$$\partial_z p^m(r,\pm h)=0, \quad \text{for } r\le a. \tag{3.33b}$$

The functions $q^m(r,z)$ are the Fourier expansion coefficients of the source $q(r,z,\phi)$, with $q^0(r,z)$ satisfying the compatibility condition

$$\int_0^a\int_{-h}^h q^0(r,z)\,r\,dr\,dz=0. \tag{3.34}$$

The dependence on r is defined employing a basis similar to the one proposed for the radial direction in polar coordinates by Matsushima and Marcus [17], see also Verkley [18]. Reminding the definition of the dimensionless variables $\rho=r/a$, with $0<\rho\leq 1$, and $\zeta=z/h$, with $|\zeta|\leq 1$, we introduce the expansion functions, for $m\geq 0$,

$$\hat{B}_{\hat{\imath}}^{m}(\rho)=\rho^{m}\hat{P}_{\hat{\imath}}^{(0,m)}(2\rho^{2}-1), \tag{3.35}$$

where $\hat{P}_{\hat{\imath}}^{(0,m)}(s)$ are the normalized Jacobi polynomials defined in [21].

The basis $\hat{L}_{\hat{\jmath}}(\zeta)$ used to represent the dependence on the axial variable ζ consists of the *normalized* Legendre polynomials, namely,

$$\hat{L}_{\hat{\jmath}}(\zeta)\equiv\sqrt{\hat{\jmath}+\frac{1}{2}}\,L_{\hat{\jmath}}(\zeta),\quad \text{for } \hat{\jmath}\geq 0, \tag{3.36}$$

where $L_{\hat{\jmath}}(\zeta)$, $\hat{\jmath}\geq 0$, are the Legendre polynomials.

The spectral approximation to $p^{m}(\rho,\zeta)$ is defined by

$$p^{m}(\rho,\zeta)=\sum_{\hat{\imath}=0}^{N-|m|}\hat{B}_{\hat{\imath}}^{|m|}(\rho)\,\hat{p}_{\hat{\imath};\hat{\jmath}}^{m}\hat{L}_{\hat{\jmath}}(\zeta)\sum_{\hat{\jmath}=0}^{\hat{J}}. \tag{3.37}$$

By using the Galerkin method, the discrete form of the Poisson-Neumann problem consists of the following linear system of equations, for $-N+1\leq m\leq N$,

$$a^{-2}\hat{D}_{\boxed{m}}\hat{P}^{m}+\hat{P}^{m}\hat{D}h^{-2}=\hat{Q}^{m}, \tag{3.38}$$

where

$$\hat{P}^{m}=\{\hat{p}_{\hat{\imath},\hat{\jmath}}^{m},\ 0\leq\hat{\imath}\leq N-|m|,\ 0\leq\hat{\jmath}\leq\hat{J}\}. \tag{3.39}$$

For the first mode $m=0$ matrix $\hat{D}_{\boxed{0}}$ is singular. Since also matrix $\hat{D}$ is (always) singular, the singularity of the linear system (3.38) for $m=0$ implies that the unknown $\hat{P}^{0}$ is indeterminate by an arbitrary additive constant. This is in conformity with the presence of the compatibility condition satisfied by q^{0}. For details about the expression of the matrices $\hat{D}_{\boxed{m}}$, $\hat{D}$ and of the array $\hat{Q}^{m}$, see [21]. The linear systems (3.38) are solved by double diagonalization.

4 Evaluation of the explicit terms

To complete the description of the algorithm for the spectral simulation of incompressible flows it is necessary to show how the explicit terms of the equations are evaluated. In the momentum equation two terms, the pressure gradient and the nonlinear term, must be considered, while in the pressure Poisson equation only a divergence term must be evaluated. In the proposed method all these terms, expressed in weak form, are calculated

by a pseudospectral technique, which requires to introduce the following sets of points along the three cylindrical "directions":

$$r_g = \left(\frac{1+s_g}{2}\right)^{\frac{1}{2}}, \qquad 1 \le g \le N+1, \tag{4.1}$$

$$z_\ell = h\zeta_\ell, \qquad 1 \le \ell \le J+1, \tag{4.2}$$

$$\phi_k = \frac{(k-1)\pi}{N}, \qquad 1 \le k \le 2N, \tag{4.3}$$

where s_g are Gauss-Legendre quadrature points over the interval $|s| \le 1$ and similarly the points ζ_ℓ over the interval $|\zeta| \le 1$.

The pseudospectral technique amounts to the following two steps:

1. Compute the point values of the required term (gradient, divergence, nonlinear);
2. L^2 project the term on the basis functions by Fourier transform and Gaussian quadrature.

The two steps are performed by standard techniques, so that it will suffice to give here only the essential elements required by the present method.

A scalar function $u = u(r,z,\phi)$ defined over the cylinder will be represented either by its expansion coefficients, organized in the structured three-dimensional array,

$$\boldsymbol{U} = \left\{ u_{i,j}^m,\ 0 \le i \le N-|m|,\ 0 \le j \le J,\ -N+1 \le m \le N \right\}, \tag{4.4}$$

or by the three-dimensional rectangular array

$$\boldsymbol{\mathcal{U}} = \left\{ u(r_g, z_\ell,\ \phi_k),\ 1 \le g \le N+1,\ 1 \le \ell \le J+1,\ 1 \le k \le 2N \right\}, \tag{4.5}$$

of its point values over the aforementioned cylindrical grid.

The point values $\boldsymbol{\mathcal{U}}$ are computed from the expansion coefficients $\boldsymbol{U}$ by the following transformation

$$\boldsymbol{\mathcal{U}} = \mathbb{F}^{-1}\Big(\mathbb{L}\left(\mathbb{B}\left(\boldsymbol{U}\right)\right)\Big), \tag{4.6}$$

where $\mathbb{F}$ denotes the Fourier transform and $\mathbb{L}$ and $\mathbb{B}$ amount to multiply each coefficient by the value assumed by the corresponding basis functions, Legendre axial basis functions and radial basis functions respectively, on the Gauss points.

The L^2 projection of the point values $\boldsymbol{\mathcal{U}}$ onto the basis functions requires to introduce the weights v_g and w_ℓ of the Gauss-Legendre quadrature formula with $N+1$ and $J+1$ points, respectively. One has

$$\boldsymbol{U} = \frac{1}{4}\mathbb{B}_G\Big(\mathbb{L}_G\left(\mathbb{F}\left(\boldsymbol{\mathcal{U}}\right)\right)\Big), \tag{4.7}$$

where the operators $\mathbb{B}_G$ and $\mathbb{L}_G$ include the multiplication by the appropriate weights of the Gaussian quadrature and by the point values of the basis functions. Transformations $\mathbb{L}$, $\mathbb{L}_G$, $\mathbb{B}$, $\mathbb{B}_G$ are actually performed by matrix-matrix multiplications.

We analyze first the transformations needed to evaluate the nonlinear term. The transformations for vector fields in cylindrical coordinates are more complicated since point values are required for the *cylindrical components* of the velocity field, which are indicated by u_r,u_ϕ and u_z, to give

$$\vec{\boldsymbol{\mathcal{U}}} = (\boldsymbol{\mathcal{U}},\boldsymbol{\mathcal{V}},\boldsymbol{\mathcal{W}}) = (\boldsymbol{\mathcal{U}}_r,\boldsymbol{\mathcal{U}}_\phi,\boldsymbol{\mathcal{U}}_z), \tag{4.8}$$

whereas the structured arrays of the expansion coefficients are known for the *uncoupled components* u_1,u_2 and $u_3 = u_z$, denoted collectively as

$$\vec{\boldsymbol{U}} = (\boldsymbol{U}_1,\boldsymbol{U}_2,\boldsymbol{U}_3). \tag{4.9}$$

These two sets of vector components are related by the transformation operator $\mathbb{Q}$ defined in Section 3.2, which is acting in the space of the Fourier coefficients of the velocity components. By taking into account the role of the uncoupling transformation $\mathbb{Q}$, the transformations for the velocity vector variable and the L^2 projection of the nonlinear term will be indicated formally as

$$\vec{\boldsymbol{\mathcal{U}}} = \mathbb{F}^{-1}\big(\mathbb{Q}^{-1}\big(\mathbb{L}\,(\mathbb{B}\,(\vec{\boldsymbol{U}}))\big)\big), \quad \text{and} \quad \vec{\boldsymbol{N}} = \frac{1}{4}\mathbb{B}_G\Big(\mathbb{L}_G\big(\mathbb{Q}(\mathbb{F}\,(\vec{\boldsymbol{\mathcal{N}}}))\big)\Big), \tag{4.10}$$

respectively. The evaluation of the nonlinear term $(\boldsymbol{u}\cdot\boldsymbol{\nabla})\boldsymbol{u}$ in weak form proceeds as follows. First transform the expansion coefficients $\vec{\boldsymbol{U}}$ of the uncoupled velocity components to the values $\vec{\boldsymbol{\mathcal{U}}}$ of the cylindrical components in the physical space by means of

$$\vec{\boldsymbol{\mathcal{U}}} = \mathbb{F}^{-1}\Big(\mathbb{Q}^{-1}\big(\mathbb{L}\,(\mathbb{B}\,(\vec{\boldsymbol{U}}))\big)\Big). \tag{4.11}$$

Second, evaluate the derivatives $\boldsymbol{\mathcal{U}}_{\partial r}$, $\boldsymbol{\mathcal{U}}_{\partial z}$ and $\boldsymbol{\mathcal{U}}_{\partial\phi}$, and similarly for the other two cylindrical components $\boldsymbol{\mathcal{V}}$ and $\boldsymbol{\mathcal{W}}$. This requires to know the point values of the derivative of the radial basis functions, namely, $dB_i^\ell(r_g)/ds$, and of the basis functions $L_j^*(\zeta)$, namely, $dL_j^*(\zeta_\ell)/d\zeta$.

Then determine the cylindrical components of the nonlinear term $(\boldsymbol{u}\cdot\boldsymbol{\nabla})\boldsymbol{u}$ through the expressions

$$\boldsymbol{\mathcal{N}}_r = \boldsymbol{\mathcal{U}}\star\boldsymbol{\mathcal{U}}_{\partial r} + (a\mathcal{R})^{-1}\boldsymbol{\mathcal{V}}\star(\boldsymbol{\mathcal{U}}_{\partial\phi} - \boldsymbol{\mathcal{V}}) + \boldsymbol{\mathcal{W}}\star\boldsymbol{\mathcal{U}}_{\partial z}, \tag{4.12a}$$

$$\boldsymbol{\mathcal{N}}_\phi = \boldsymbol{\mathcal{U}}\star\boldsymbol{\mathcal{V}}_{\partial r} + (a\mathcal{R})^{-1}\boldsymbol{\mathcal{V}}\star(\boldsymbol{\mathcal{V}}_{\partial\phi} + \boldsymbol{\mathcal{U}}) + \boldsymbol{\mathcal{W}}\star\boldsymbol{\mathcal{V}}_{\partial z}, \tag{4.12b}$$

$$\boldsymbol{\mathcal{N}}_z = \boldsymbol{\mathcal{U}}\star\boldsymbol{\mathcal{W}}_{\partial r} + (a\mathcal{R})^{-1}\boldsymbol{\mathcal{V}}\star\boldsymbol{\mathcal{W}}_{\partial\phi} + \boldsymbol{\mathcal{W}}\star\boldsymbol{\mathcal{W}}_{\partial z}, \tag{4.12c}$$

where $\star$ denotes the element-by-element multiplication of arrays and where we have introduced the diagonal matrix

$$\mathcal{R} \equiv \mathrm{diag}\big(r_g,\, 1 \le g \le N+1\big). \tag{4.13}$$

We notice that the left multiplication by $\mathcal{R}^{-1}$ must be done on any column and for any plane $k = \text{constant}$ of the subsequent 3D array. Finally evaluate the L^2 projection of the

nonlinear term by means of

$$\vec{\boldsymbol{N}}=\frac{1}{4}\mathbb{B}_G\Big(\mathbb{L}_G\big(\mathbb{Q}(\mathbb{F}(\vec{\boldsymbol{\mathcal{N}}}))\big)\Big). \tag{4.14}$$

The evaluation of the gradient term proceeds along the same lines. From the expansion coefficients

$$\hat{\boldsymbol{P}}=\Big\{\hat{p}^m_{\hat{\imath},\hat{\jmath}},\ 0\le\hat{\imath}\le N-|m|,\ 0\le\hat{\jmath}\le\hat{J},\ -N+1\le m\le N\Big\}, \tag{4.15}$$

of the pressure, one first evaluates the cylindrical components of its gradient in the Fourier space, but at the grid points (r_g,z_ℓ), i.e., $\mathbb{F}^{-1}$ is omitted. Then, the transformation $\mathbb{Q}$ is applied to yield the gradient components in the uncoupled basis. Finally, the term is projected to give its contribution to the momentum equation in weak form.

The divergence of velocity is evaluated by first transforming the expansion coefficients $\vec{\boldsymbol{\mathcal{U}}}$ into the values at the grid points (r_g,z_ℓ), and obtaining also the corresponding derivatives with respect to r and z. Then, the transformation $\mathbb{Q}^{-1}$ is applied to obtain the cylindrical velocity components and their derivatives. Finally, the expression of divergence is evaluated and projected to have the weak term contributing to the right-hand side of the scalar pressure equation.

5 Removal of corner singularity

Typical velocity boundary conditions for flow problems in cylindrical cavities involve a discontinuous distribution of the boundary values of some component where the bottom or top walls touch the lateral side. For instance, in the axisymmetric flow within a cylinder driven by the rotation of the top side with angular velocity Ω around the axis, the angular component of velocity is prescribed to vanish on the lateral curved surface but also to be $a\Omega$ at the external limit of the circular top side. Thus the boundary value to be imposed on u_ϕ is discontinuous in the corner (a,h). As well known, such a discontinuity prevents the solution u_ϕ to belong to the Sobolev space $H^1(\Omega)$ so that it is necessary to remove it, especially in the context of a spectral approximation to the governing equations. We describe a method to remove the corner singularity. The method is the simple adaptation to cylindrical coordinates of the technique already applied in the spectral solution of the 3D driven cavity problem [28].

Let us consider the following axisymmetric elliptic boundary value problem

$$\begin{cases}\Big(-\partial_0^2+\dfrac{1}{r^2}+\gamma\Big)u=f(r,z),\\ u(r,h)=\Omega r, & r\le a,\\ u(a,z)=0, & |z|\le h,\\ u(r,-h)=0, & r\le a.\end{cases} \tag{5.1}$$

In the spectral solution of this singular problem, the boundary value imposed at the discontinuous corner is the average of the two different values, namely, $u(a,h)=a\Omega/2$.

To regularize such a discontinuity in the boundary values at the upper-right corner (a,h) we introduce the function

$$\psi(r,z)=\begin{cases}1-\dfrac{2}{\pi}\tan^{-1}\Big(\dfrac{h-z}{a-r}\Big), & 0\le r<a, \quad z\le h,\\ 0, & r=a, \quad z\le h.\end{cases} \tag{5.2}$$

The unknown variable u is replaced by the "nonsingular" unknown v defined such as

$$u=v+S, \tag{5.3}$$

where $S(r,z)\equiv\Omega r\psi(r,z)$ inside the rectangular domain of the problem. In this way the condition of differentiability to all orders of the original unknown $u=u_\phi$ for the axisymmetric problem is satisfied also by the new variable. The new unknown v is solution of the "desingularized" boundary value problem:

$$\begin{cases}\Big(-\partial_0^2+\dfrac{1}{r^2}+\gamma\Big)v=g(r,z), & \\ v(r,h)=0, & r\le a,\\ v(a,z)=0, & |z|\le h,\\ v(r,-h)=-\Omega r\psi(r,-h), & r\le a,\end{cases} \tag{5.4}$$

where

$$g(r,z)\equiv f(r,z)-\frac{6\Omega}{\pi}\frac{h-z}{(a-r)^2+(h-z)^2}-\gamma\Omega r\psi(r,z). \tag{5.5}$$

The application of this technique to the Navier-Stokes problem with one or two rotating lids is immediate. Supposing that only the top lid is rotating with angular velocity Ω, one introduces the modified velocity field $\boldsymbol{v}(\boldsymbol{r},t)$, as the new unknown, by means of the definition

$$\boldsymbol{u}(\boldsymbol{r},t)=\boldsymbol{v}(\boldsymbol{r},t)+\Omega r\psi(r)\hat{\boldsymbol{\phi}}. \tag{5.6}$$

It follows that the initial and boundary conditions for the nonsingular unknown $\boldsymbol{v}$ read

$$\boldsymbol{v}(\boldsymbol{r},0)=\boldsymbol{u}_0(\boldsymbol{r})-\Omega r\psi(r)\hat{\boldsymbol{\phi}}, \tag{5.7a}$$

$$\boldsymbol{v}(\boldsymbol{r},t)|_{\partial\Omega}=\boldsymbol{b}(\boldsymbol{r}_{\partial\Omega},t)-\Omega[r\psi(r)]|_{\partial\Omega}\hat{\boldsymbol{\phi}}. \tag{5.7b}$$

The elliptic equation for the angular component of velocity will be modified by augmenting its right-hand side with the additional source term $-6\Omega(h-z)/\pi\big((a-r)^2+(h-z)^2\big)$.

Finally, the nonlinear vector term will be evaluated by replacing the angular component of the velocity $\boldsymbol{\mathcal{V}}$ with the sum $\boldsymbol{\mathcal{V}}+\boldsymbol{\mathcal{S}}$, where $\boldsymbol{\mathcal{S}}$ denotes the values of the singular function

$$S(r,z)=\Omega r\psi(r,z) \tag{5.8}$$

at the Gauss points. Thus the nonlinear term of the desingularized velocity equation becomes

$$\begin{pmatrix} \mathcal{N}_r \\ \mathcal{N}_\phi \\ \mathcal{N}_z \end{pmatrix} = \begin{pmatrix} \mathcal{U}\star\mathcal{U}_{\partial r}+(a\mathcal{R})^{-1}(\mathcal{V}+\mathcal{S})\star(\mathcal{U}_{\partial\phi}-\mathcal{V}-\mathcal{S})+\mathcal{W}\star\mathcal{U}_{\partial z} \\ \mathcal{U}\star(\mathcal{V}_{\partial r}+\mathcal{S}_{\partial r})+(a\mathcal{R})^{-1}(\mathcal{V}+\mathcal{S})\star(\mathcal{V}_{\partial\phi}+\mathcal{U})+\mathcal{W}\star(\mathcal{V}_{\partial z}+\mathcal{S}_{\partial z}) \\ \mathcal{U}\star\mathcal{W}_{\partial r}+(a\mathcal{R})^{-1}(\mathcal{V}+\mathcal{S})\star\mathcal{W}_{\partial\phi}+\mathcal{W}\star\mathcal{W}_{\partial z} \end{pmatrix}, \quad (5.9)$$

where $\mathcal{U},\mathcal{V}$ and $\mathcal{W}$ are the 3D arrays of values at Gauss points of the cylindrical components of the nonsingular unknown $\boldsymbol{v}$.

Notice that in the viscous problem for the vector velocity the desingularization procedure regards the full Navier-Stokes problem, not a single uncoupled scalar elliptic equation, since evaluation of the nonlinear term (5.9) involves the singular function $S(r,z)=\Omega r\psi(r,z)$. It must be remarked that the procedure for desingularizing the problem can be implemented in the proposed method thanks to the fact that no quadrature point lies on the boundary and that the derivatives $\mathcal{S}_{\partial r}$ and $\mathcal{S}_{\partial z}$, needed in (5.9), are evaluated only at internal points of the rectangle $[0,a]\times[-h,h]$ where they are finite.

We have solved the Navier-Stokes problem with $\mathrm{Re}=10$ in the cylinder $[0,a]\times[-h,h]$, for a=1.5 and h=1, with the bottom lid rotating. Spectral discretizations with $N=J$=16,24 and 32 have been considered, with the LBB condition respected both in the radial and axial directions. The former condition is fulfilled by suppressing the last radial basis function of the first Fourier mode $m=0$ of pressure, as detailed in the next section. The solutions without desingularization are compared with a reference spectral solution to the desingularized problem with $N=J=64$ by evaluating the relative L^2 and L^∞ errors of the azimuthal velocity component, which are reported in Table 1.

Table 1: Relative L^2 and L^∞ errors of u_ϕ for the spectral solutions without desingularization, second and fourth column, and with desingularization, third and fifth column. The error is calculated with respect to a reference spectral solution to the desingularized problem with $N=J=64$. In all cases the LBB condition is respected. The domain is the cylinder $r\le 1.5$, $|z|\le 1$.

$N=J$	L^2	L^2	L^∞	L^∞
16	1.4×10^{-2}	1.7×10^{-4}	5.4×10^{-1}	1.9×10^{-3}
24	6.4×10^{-3}	4.2×10^{-5}	4.0×10^{-1}	8.2×10^{-4}
32	3.6×10^{-3}	1.6×10^{-5}	3.9×10^{-1}	3.8×10^{-4}

We note that the singular solution u_ϕ converges in the L^2 norm but presents local errors which are almost constant as witnessed by the L^∞ error. On the contrary, the desingularized solution displays a faster convergence rate and a more uniform distribution of the error as shown by the errors in the two considered norms. As far as the other velocity components are concerned, the accuracy of the singular and desingularized solutions is almost identical at the considered Reynolds number.

A plot of the difference between the solutions to the singular and desingularized problems is provided in Fig. 2 in terms of the level curves $\Delta u_\phi=0,\pm10^{-2},\pm10^{-3}$ and $\pm10^{-4}$, for $N=J=16$. The maximum difference is 0.27 and located in the lower right corner of the section of the cylindrical domain. The strongest spatial oscillations are located

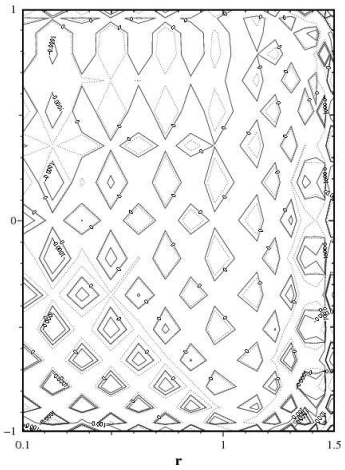

Figure 2: Difference between the spectral solutions u_ϕ, with and without the desingularization technique.

in this corner and along the two intersecting sides but are of an appreciable intensity throughout the entire computational domain, as clearly illustrated in Fig. 2.

6 Numerical tests

Several numerical solutions have been computed to validate the Navier-Stokes solver. First of all, our solution is shown to agree with an exact steady-state solution of the flow equations and the fundamental importance of satisfying the LBB condition is also documented. Then the time accuracy of the numerical scheme is assessed by considering a time-dependent analytical solution of the Navier-Stokes equations. We finally test our solver against well documented solutions available in the literature: an axisymmetric flow with bubble formation and a fully 3D flow exhibiting rotating waves.

6.1 Convergence to steady-state solution and LBB condition

To test the spatial convergence of the Navier-Stokes solver, an exact steady-state solution to the nonlinear equations is taken in the following form

$$u_x(x,y,z)=(\sin x)(\cos y)(\sin z), \qquad u_y(x,y,z)=(\cos x)(\sin y)(\sin z),$$
$$u_z(x,y,z)=2(\cos x)(\cos y)(\cos z), \qquad p(x,y,z)=\frac{3}{\mathrm{Re}}(\cos x)(\cos y)(\cos z).$$

The 3D Cartesian velocity field above is solenoidal and the Cartesian-coordinate-based problem above represents a quite general test for the cylindrical spectral solver. The corresponding source term is calculated analytically and the steady numerical solution is

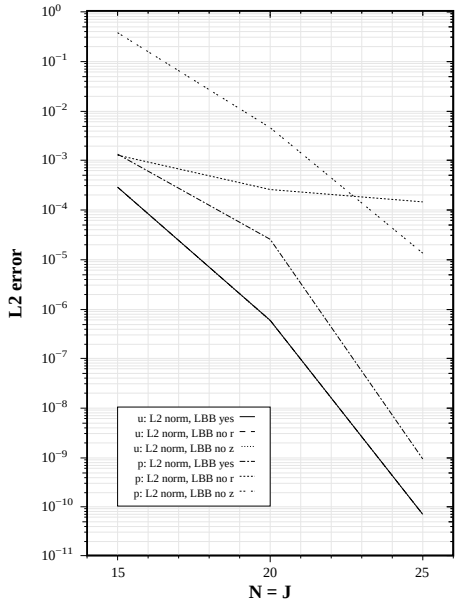

Figure 3: Convergence rate of the spatial discretizations respecting or violating the LBB condition. The three curves of the velocity errors are almost identical and they collapse in the single continuous curve which is the lowest of the plot.

compared with the exact one after the velocity is transformed in cylindrical components. The error is evaluated using the weighted $L^2_r(\Omega)$ norm, defined by

$$L^2_r\text{error} = \|u_{\text{computed}} - u_{\text{exact}}\|_{L^2_r},$$

where

$$\|u\|^2_{L^2_r} = \int_0^a \int_{-h}^h \int_0^{2\pi} [u(r,z,\phi)]^2 r dr dz d\phi.$$

The L^2_r norm of a vector function is defined in the standard way by

$$\|\boldsymbol{u}\|^2_{L^2_r} = \|u_r\|^2_{L^2_r} + \|u_\phi\|^2_{L^2_r} + \|u_z\|^2_{L^2_r},$$

which allows the definition of the corresponding L^2_r error of the velocity spectral solution. In Fig. 3 we plot the error for three spectral discretizations with $N = J = 15,20,25$ for the velocity field. The computational domain is the cylinder with $a = 6$ and $h = 4$ and the Reynolds number is $\text{Re} = 10$.

For the incompressible equations the spatial discretization of the pressure is known to be subject to a stability constraint, called LBB condition. When this condition is violated, spurious pressure modes appear in the computed pressure field. Moreover, for spatial discretization of local type, such as finite elements or differences, unphysical spatial oscillations are generated also in the velocity field, provided the time-step is sufficiently small.

The situation is slightly different for approximations of global type, such as the spectral method, of interest here. It has been found in [27] for Galerkin Legendre approximations to the Cartesian Navier-Stokes equation that the violation of LBB condition produces spurious spatial oscillations, but only in the pressure field while the convergence of the velocity is unaffected. In any case the development of spurious pressure mode is prevented in the spectral solution simply by using a polynomial representation for the pressure of two degrees lower than that used for the velocity. This treatment must be adopted for the spatial discretization in each space direction with two boundary conditions.

In the present case of cylindrical domain with one periodic direction, the LBB condition can be violated when choosing the bases to represent either the axial dependence or the radial dependence or both. For the former direction, the LBB stability condition is satisfied simply by taking $\hat{J}=J-2$. For the latter, radial, direction the required modification in the radial expansion can be obtained instead by reducing the dimension only of the subspace of the mode $m=0$. The expansion in Jacobi polynomials in this subspace is easily reduced by eliminating only the highest mode. The complete expansion of the pressure field including the order reduction to satisfy the LBB stability condition both in the radial and axial direction would therefore read:

$$p(\rho,\zeta,\phi)=\sum_{\hat{\imath}=0}^{N-1}\hat{B}_{\hat{\imath}}^{0}(\rho)\,\hat{p}_{\hat{\imath},\hat{\jmath}}^{0}\,\hat{L}_{\hat{\jmath}}(\zeta)\sum_{\hat{\jmath}=0}^{\hat{J}}+2\sum_{m=1}^{N-1}\Big[\sum_{\hat{\imath}=0}^{N-m}\rho^{m}\,\hat{B}_{\hat{\imath}}^{m}(\rho)\,\hat{p}_{\hat{\imath},\hat{\jmath}}^{\pm m}\,\hat{L}_{\hat{\jmath}}(\zeta)\sum_{\hat{\jmath}=0}^{\hat{J}}\Big]\begin{matrix}\cos(m\phi)\\-\sin(m\phi)\end{matrix}$$
$$+\rho^{N}\Big[\hat{p}_{0,\hat{\jmath}}^{N}\,\hat{L}_{\hat{\jmath}}(\zeta)\sum_{\hat{\jmath}=0}^{\hat{J}}\Big]\cos(N\phi).$$

We compare the errors of pressure and velocity obtained by means of the Navier-Stokes spectral solver including three different treatments of the LBB condition: the first spectral approximation fulfills the LBB condition both in the axial and radial direction; the second approximation violates the LBB condition only for the radial expansion; finally, the third approximation violates the LBB condition only for the axial expansion.

The convergence curves of the velocity error are given in Fig. 3. The computational domain is the cylinder with $a=6$ and $h=4$. The three curves are almost identical and appear as the single lowest line in the plot. Therefore, the spectral convergence of velocity field is achieved irrespective of the satisfaction or violation of the LBB condition.

On the contrary, the pressure error depends on whether LBB condition is satisfied or not and three different curves indicate that only when the LBB constraint is respected the convergence of the computed pressure field to the exact pressure can be assured. The other two schemes with only a partial fulfillment of the stability condition cannot converge with spectral accuracy even though the solution of the velocity field does.

The violation of the stability condition in the axial expansion is more severe than that in radial direction. However, the latter violation also prevents spectral convergence. In Fig. 4 the difference between exact and computed pressure is shown for the LBB correct

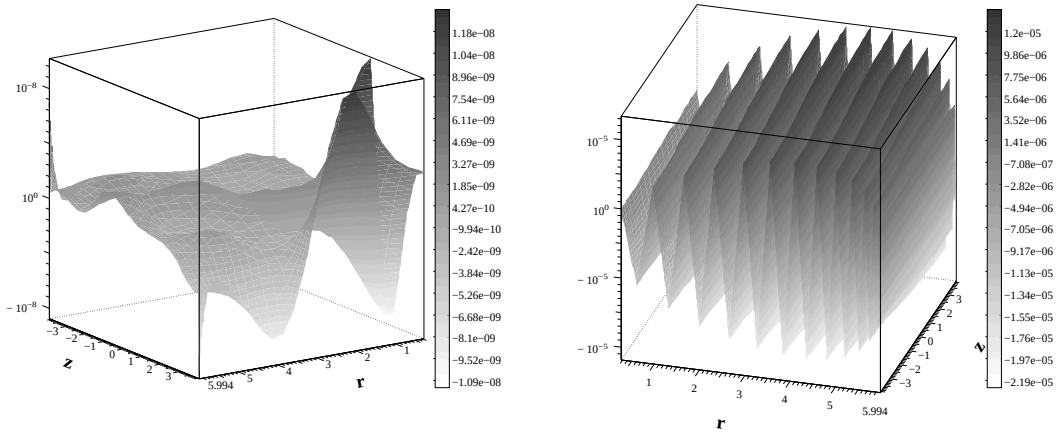

Figure 4: Pressure error and fulfillment of the LBB stability condition, for $N=J=25$ and $\hat{J}=23$. Left: LBB fully satisfied; Right: LBB *not* satisfied in the radial direction.

method (left plot) and for the method violating LBB only radially (right plot), for the steady-state spectral solution with $N=J=25$ and $\hat{J}=23$. In the right plot the spatial oscillations in an axial plane are clearly seen and are of the same nature in any other axial plane. By contrast the pressure error of the LBB-correct method shown in the left plot is three orders of magnitude smaller, is free from spurious spatial oscillations and displays the spectral rate of convergence.

6.2 Time accuracy of the BDF solver

To assess the convergence rate of the algorithm with respect to the step-size we have taken a transient analytical solution defined as follows. Consider the stationary 2D velocity field

$$u_x^{\rm s}(x,z)=-\cos x\sin z,\qquad u_z^{\rm s}(x,z)=\sin x\cos z,$$

which develops in the vertical plane x-z and is solenoidal. The time-dependent velocity field solution to the unsteady Navier-Stokes equations in three dimensions and the corresponding source terms are given by

$$\boldsymbol{u}(\boldsymbol{r},t)=\boldsymbol{u}^{\rm s}(x,z)g(t),\qquad \boldsymbol{f}(\boldsymbol{r},t)=\boldsymbol{u}^{\rm s}(x,z)\left[g'(t)+\frac{2g(t)}{\rm Re}\right],$$

with $u_y=0$ and $f_y=0$. The pressure field of this time-dependent solution is given by

$$p(x,z,t)=-\frac{1}{4}\left[\cos(2x)+\cos(2z)\right]g^2(t).$$

We assume $g(t)=\sin^2 t$. This Cartesian velocity field is transformed in cylindrical components u_r,u_ϕ and u_z to test the Navier-Stokes spectral solver inside the cylinder. The velocity boundary values are determined from the exact unsteady solution as $\boldsymbol{b}=\boldsymbol{u}(r,z,\phi,t)_{|\partial\Omega}$.

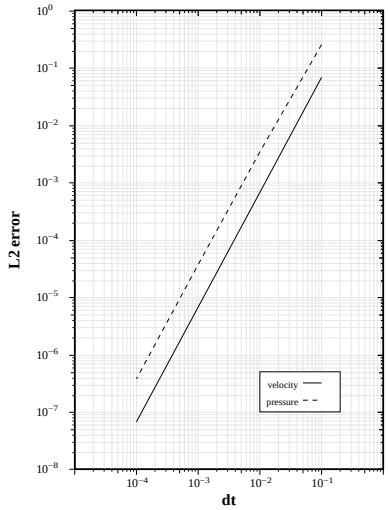

Figure 5: Convergence rate of time discretization, for $N=J=25$, $\hat{J}=23$ and LBB condition fulfilled.

Similarly, the initial velocity field is taken as

$$\boldsymbol{u}_0(\boldsymbol{r})=\boldsymbol{u}(\boldsymbol{r},0)=\boldsymbol{u}^{\mathrm{s}}(\boldsymbol{r})g(0)=0.$$

Finally, the initial pressure field required by the second-order incremental BDF scheme is taken as $p_0(\boldsymbol{r})=p(\boldsymbol{r},0)=0$. The temporal convergence is measured in the norm $l^\infty(0,T;L^2)$.

In Fig. 5 the $l^\infty(1,2;L^2)$ errors of the spectral solutions for $N=J=25$, fulfilling the LBB condition, over the computational domain $a=6$ and $h=4$ for $\mathrm{Re}=10$ are reported as a function Δt. The expected $\mathcal{O}(\Delta t^2)$ accuracy of the second-order BDF time integration scheme with a full respect of the LBB stability condition is confirmed.

6.3 Axisymmetric bubble formation

We consider the rotor-stator configuration with aspect ratio $2h/a=2$ at $\mathrm{Re}=1850$, for which Daube [29] found numerically a steady-state solution characterized by two recirculation bubbles, located on the axis at $z=0$ and $z=0.5$, approximately. This flow was also investigated experimentally by Escudier [30].

The spectral solution has been obtained setting $N=J=48$ and fulfilling the LBB condition. In Fig. 6 the streamlines of the velocity vector field in the axial plane are shown, which compare well with the contours of the Stokes streamfunction previously computed by Daube [29]. Note that this solution is also similar to the steady-state solution computed by Lopez and Shen [6] for $\mathrm{Re}=2494$ and for the slightly larger aspect ratio $2h/a=2.5$.

A more quantitative comparison is made by superimposing the distribution of the axial velocity u_z on the cylinder axis obtained by Daube, using a vorticity-velocity formulation, and with the present method. As shown in Fig. 7 there is a very good agreement

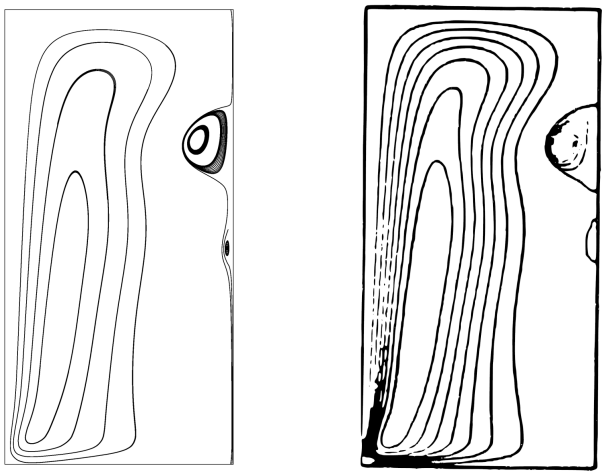

(a) (b)

Figure 6: (a) Streamlines of the velocity vector field obtained from the present Navier-Stokes solver. (b) Contours of the Stokes streamfunction from [29].

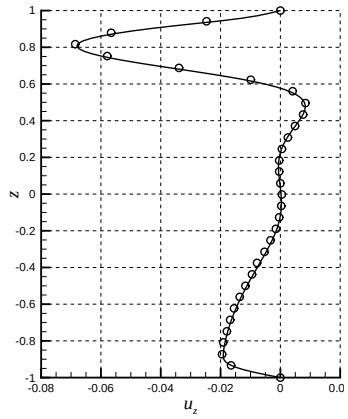

Figure 7: Distribution of the axial velocity on the cylinder axis obtained using the present method (continuous line) and from [29] (○).

between the profiles of u_z and, in particular, between the predicted position of the two recirculation bubbles.

6.4 3D flow with rotating waves

The capability of the Navier-Stokes solver to represent correctly the dynamics of a purely three-dimensional flow has been assessed by reproducing the onset of rotating waves in a rotor-stator configuration for $2h/a = 1.72$ and $\mathrm{Re} = 4500$.

The flow under investigation exhibits a complex nonlinear spatial structure, as may be deduced from Fig. 8, where the contours of the radial velocity component u_r are plotted in

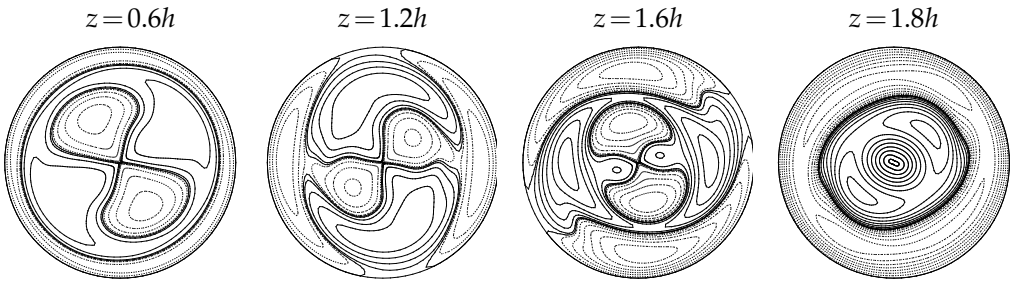

Figure 8: Contour lines of the radial component u_r of the velocity vector for different distances $\overline{z}$ from the bottom end wall.

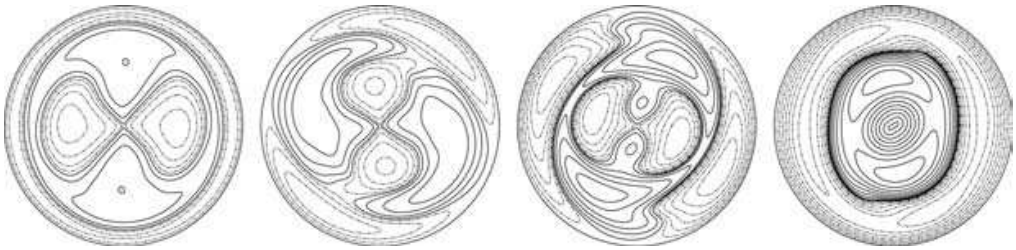

Figure 9: Contour lines of the radial component u_r of the velocity vector for different distances $\overline{z}$ from the bottom end wall from Lopez [31].

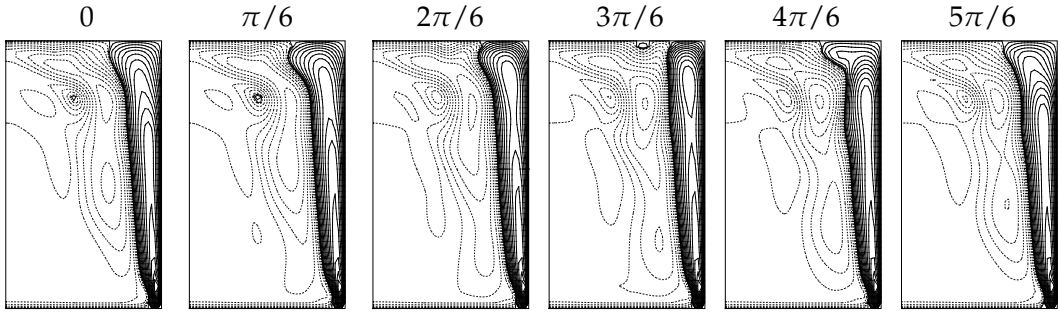

Figure 10: Contour lines of the axial component u_z of the velocity vector at different azimuthal angles.

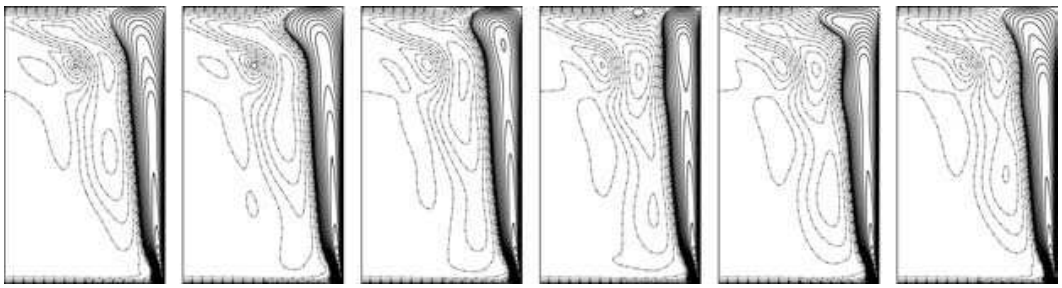

Figure 11: Contour lines of the axial component u_z of the velocity vector at different azimuthal angles, from Lopez [31].

planes at different distances from the bottom wall. These contours rotate rigidly around the cylinder axis with a constant angular velocity and in the same direction of the rotating end wall. Analyzing Fig. 8 it is also clearly seen that the flow has a spatial symmetry $Z_2 = \{\mathbf{1}, R_\pi\}$. There is an excellent match between the presented solution and that presented in Lopez [31] reported here in Fig. 9.

Fig. 10 presents the contour lines of the axial velocity u_z in planes at various azimuthal angle $\phi \in [0, \pi)$. Inspecting the contours at $\phi = 3\pi/6$, the presence of two small spiral separation zones may be clearly seen near the fixed top wall. The same structures can be observed also in the reference solution reported in Fig. 11.

7 Conclusions

A new primitive variable spectral method for simulating incompressible viscous flows inside a finite cylinder has been presented. The solver is based on the Galerkin formulation of a second-order BDF projection method for the Navier-Stokes equations in cylindrical coordinates. The velocity and pressure fields have been expanded using one-sided Jacobi polynomials with a parabolically stretched variable for representing the radial structure of the solution and Legendre polynomials for its axial dependence, combined with Fourier analysis. Apart from the Fourier representation which is common to the velocity and pressure fields, different bases are adopted for expanding the pressure and velocity fields.

The pressure is advanced in time by a scalar Poisson equation with Neumann boundary condition and is expanded in normalized Jacobi and Legendre polynomials. While the latter expansion for the axial coordinate is one and the same for all Fourier modes the former expansion for the radial variable has a size decreasing with the Fourier modal index. As a consequence, the number of radial modes involved is minimal and the discrete approximation does not introduce an artificial clustering of the integration points close to the centre, present instead in other spectral methods. The matrices representing the differential operators in the radial and axial directions are full and the solution of the discrete pressure equations of each Fourier mode are calculated by means of double diagonalization.

Coming to the velocity, this field is advanced in time by a Helmholtz equation supplemented by Dirichlet condition and is expanded on a basis constructed from Jacobi polynomials different from that used for the pressure and which has been introduced recently by two of the present authors [21]. As far as the dependence on the axial coordinate is concerned, the basis for velocity is built on Legendre polynomials as proposed by Jie Shen for a Cartesian coordinate. The radial discretization of the velocity is of a different order depending on the Fourier modal index m, with the same decrease at higher m occurring for the pressure. Moreover, the discrete representation of the radial differential operators is optimal since the matrix corresponding to the second radial derivative is diagonal and that corresponding to the mass matrix is tridiagonal, for all Fourier modes. In

this sense the solution algorithm for the Dirichlet problem represents the true extension to cylindrical coordinates of the algorithms introduced by Shen for elliptic equations in Cartesian coordinates. The sparse structure of the matrices for both the radial and axial operators leads to eigenvalue problems for very simple matrices in the construction of the double diagonalization algorithm for solving the velocity equation.

By summarizing, the spectral solver for the Navier-Stokes problem in a finite cylindrical domain is a purely variational mixed basis method without any collocation. It is also characterized by the presence of Gaussian quadrature points for evaluating the nonlinear term as well as the gradient and the divergence in weak form.

The method has been verified to be very accurate and to have the expected spectral convergence. Moreover the BDF time discretization adopted has been verified to achieve the second order accuracy for both velocity and pressure in the L_2 norm, provided the LBB condition is satisfied by a judicious but natural choice of the order of pressure interpolation, consisting in using two less spectral modes in the axial directions and one less mode in the radial direction only for the first Fourier component with $m=0$.

The comparisons with known solutions, both axisymmetric and nonaxisymmetric, as well as steady and unsteady, have shown that the proposed method is correct and reaches the spectral accuracy. Different bases are employed to expand the Fourier coefficients of pressure and velocity in the azimuthal plane. This is the only element of algorithmic complexity of the projection method which for the rest can be defined indeed truly primitive.

References

[1] R. D. Moser, P. Moin and A. Leonard, A spectral numerical method for the Navier–Stokes equations with application to Taylor–Couette flow, J. Comput. Phys., 52 (1983), 524–544.
[2] P. S. Marcus, Simulation of Taylor–Couette flow, I: numerical method and comparison with experiment, J. Fluid. Mech., 146 (1984), 45–64.
[3] P. Le Quéré an J. Pécheux, A three-dimensional pseudo-spectral algorithm for the computation of convection in a rotating annulus, Spectral and High Order Methods for Partial Differential Equations, Proceedings of the ICOSAHOM '89 Conference, Villa Olmo, Como, Italy, 26–29 June, 1989, 261–271.
[4] L. Quartapelle and M. Verri, On the spectral solution of the Navier–Stokes equations in spherical and cylindrical regions, Comput. Phys. Comm., 90 (1995), 1–43.
[5] J. M. Lopez, F. Marques and Jie Shen, An efficient spectral-projection method for the Navier–Stokes equations in cylindrical geometries, II: three-dimensional cases, J. Comput. Phys., 176 (2002), 384–401.
[6] J. M. Lopez and Jie Shen, An efficient spectral-projection method for the Navier–Stokes equations in cylindrical geometries, I: axisymmetric cases, J. Comput. Phys., 139 (1998), 308–326.
[7] Jie Shen, Efficient spectral–Galerkin methods, III: polar and cylindrical geometries, SIAM. J. Sci. Comput., 18 (1997), 74–87.
[8] H. R. Lewis and P. M. Bellan, Physical constraints on the coefficients of Fourier expansions in cylindrical coordinates, J. Math. Phys., 31 (1990), 2592–2596.

[9] B. Fornberg, A pseudospectral approach for polar and spherical geometries, SIAM. J. Sci. Comput., 16 (1995), 1071–1081.
[10] B. Fornberg, A Practical Guide to Pseudospectral Methods, Cambridge University Press, 1996.
[11] L. N. Trefethen, Spectral Methods in Matlab, SIAM, Philadelphia, 2000.
[12] M. Speetjiens and H. Clercx, A spectral solver for the Navier–Stokes equations in the velocity–vorticity formulation, Int. J. Comput. Fluid. Dyn., 19 (2005), 191–209.
[13] P. Boronski and L. S. Tuckerman, Poloidal–Toroidal decomposition in a finite cylinder, II: discretization, regularization and validation, J. Comput. Phys., 227 (2007), 1544–1566.
[14] B. Mercier and G. Raugel, Resolution d'un problème aux limites dans un ouvert axisymetrique par éléments finis en r, z et séries de Fourier en θ, R.A.I.R.O., 16 (1982), 405–461.
[15] C. Canuto, M. Y. Hussaini, A. Quarteroni and T. A. Zang, Spectral Methods in Fluid Mechanics, Springer-Verlag, New York, 1988.
[16] C. Bernardi, M. Dauge and Y. Maday, Spectral Methods for Axisymmetric Domains, Elsevier, Paris, 1999.
[17] T. Matsushima and P. S. Marcus, A spectral method for polar coordinates, J. Comput. Phys., 120 (1995), 365–374.
[18] W. T. M. Verkley, A pseudo-spectral model for two-dimensional incompressible flow in a circular basin, I: mathematical formulation, J. Comput. Phys., 136 (1997), 100–114.
[19] W. T. M. Verkley, A pseudo-spectral model for two-dimensional incompressible flow in a circular basin, II: numerical examples, J. Comput. Phys., 136 (1997), 115–131.
[20] V. G. Priymak and T. Miyazakiy, Accurate Navier–Stokes investigation of transitional and turbulent flows in a circular pipe, J. Comput. Phys., 142 (1998), 370–411.
[21] F. Auteri and L. Quartapelle, Spectral elliptic solvers in a finite cylinder, Commun. Comput. Phys., 5 (2008), 426–441.
[22] J.-L. Guermond and L. Quartapelle, Calculation of incompressible viscous flows by an unconditionally stable projection FEM, J. Comput. Phys., 132 (1997), 12–33.
[23] F. Auteri and N. Parolini, A mixed-basis spectral projection method, J. Comput. Phys., 175 (2002), 1–23.
[24] J.-L. Guermond, Un résultat de convergence d'ordre deux en temps pour l'approximation des équations de Navier-Stokes par une méthode de projection incrémentale, Modél. Math. Anal. Numér. (M^2AN), 33 (1999), 169–189.
[25] J.-L. Guermond, P. Minev and J. Shen, An overview of projection methods for incompressible flows, Comput. Meth. Appl. Mech. Eng., 195 (2006), 6011–6045.
[26] F. Auteri and L. Quartapelle, Galerkin–Legendre spectral method for the 3D Helmholtz equation, J. Comput. Phys., 161 (2000), 454–483.
[27] F. Auteri, J.-L. Guermond and N. Parolini, Role of LBB condition in weak spectral projection methods, J. Comput. Phys., 174 (2001), 405–420.
[28] F. Auteri, N. Parolini and L. Quartapelle, Simulation of 3D flows in the singular driven cavity, Report DIA SR 06-08, Politecnico di Milano, Milano, Italy, 2006.
[29] O. Daube, Resolution of the 2D Navier–Stokes equations in velocity–vorticity form by means of an influence matrix technique, J. Comput. Phys., 103 (1992), 402–414.
[30] M. P. Escudier, Observations of the flow produced in a cylindrical container by a rotating end wall, Exp. Fluids., 2 (1984), 179–186.
[31] J. M. Lopez, Rotating and modulated rotating waves in transitions of an enclosed swirling flow, J. Fluid. Mech., 553 (2006), 323–346.